Structure of a water soluble fragment of the 'Rieske' iron–sulfur protein of the bovine heart mitochondrial cytochrome bc_1 complex determined by MAD phasing at 1.5 Å resolution

So Iwata[1], Monica Saynovits[2], Thomas A Link[2] and Hartmut Michel[1]*

Background: The 'Rieske' iron–sulfur protein is the primary electron acceptor during hydroquinone oxidation in cytochrome *bc* complexes. The spectroscopic and electrochemical properties of the 'Rieske' [2Fe–2S] cluster differ significantly from those of other iron–sulfur clusters. A 129-residue water soluble fragment containing the intact [2Fe–2S] cluster was isolated following proteolytic digestion of the bc_1 complex and used for structural studies.

Results: The structure of the Rieske iron–sulfur fragment containing the reduced [2Fe–2S] cluster has been determined using the multiwavelength anomalous diffraction (MAD) technique and refined at 1.5 Å resolution. The fragment has a novel overall fold that includes three sheets of β strands. The iron atoms of the [2Fe–2S] cluster are coordinated by two cysteine (Fe-1) and two histidine (Fe-2) residues, respectively, with the histidine ligands completely exposed to the solvent. This is in contrast to the four cysteine coordination pattern observed in previously characterised [2Fe–2S] ferredoxins. The cluster-binding fold is formed by two loops connected by a disulfide bridge; these loops superpose with the metal-binding loops of rubredoxins. The environment of the cluster is stabilised by an extensive hydrogen-bond network.

Conclusions: The high-resolution structure supports the proposed coordination pattern involving histidine ligands and provides a basis for a detailed analysis of the spectroscopic and electrochemical properties. As the cluster is located at the tip of the protein, it might come into close contact with cytochrome *b*. The exposed Nε atoms of the histidine ligands of the cluster are readily accessible to quinones and inhibitors within the hydroquinone oxidation (Q_P) pocket of the bc_1 complex and may undergo redox-dependent protonation/deprotonation.

Addresses: [1]Max-Planck-Institut für Biophysik, Abt. Molekulare Membranbiologie, Heinrich-Hoffmann-Str. 7, 60528 Frankfurt/Main., Germany and [2]Universitätsklinikum Frankfurt, ZBC, Therapeutische Biochemie, D-60590 Frankfurt/M., Germany.

*Corresponding author.

Key words: cryocrystallography, cytochrome bc_1 complex, histidine ligands, multiwavelength anomalous diffraction, 'Rieske' iron–sulfur cluster

Received: 21 Feb 1996
Revisions requested: 13 Mar 1996
Revisions received: 27 Mar 1996
Accepted: 27 Mar 1996

Structure 15 May 1996, 4:567–579

 ISSN 0969-2126

Introduction

The ubiquitous cytochrome *bc* complexes are constituents of the electron transfer chains of mitochondria, chloroplasts and bacteria. All *bc* complexes contain two heme *b* centres, heme c_1 or heme *f* and a 'Rieske' iron–sulfur protein comprising a high potential [2Fe–2S] cluster. The cytochrome *bc* complexes are embedded in the respective membranes. Cytochrome *b* forms the core of the complex while cytochrome c_1/*f* and the iron–sulfur protein have their redox centres within the aqueous domain and are thought to be linked to the membrane part of the complex through hydrophobic anchors.

The Rieske iron–sulfur protein was first described and isolated by Rieske *et al.* from bovine heart bc_1 complex [1] and has later been identified as the 'oxidation factor' of the bc_1 complex [2,3]. The protein contains a [2Fe–2S] cluster showing a distinct electron paramagnetic resonance (EPR) spectrum with g_{av}=1.91 compared with g_{av}=1.96 for plant-type ferredoxins; its redox potential (+300 mV) is approximately 700 mV more positive than that of plant type [2Fe–2S] ferredoxins (–420 mV) [4]. The cluster is coordinated within a C-terminal water soluble part which is bound to the rest of the bc_1 complex probably through an N-terminal membrane anchor. Rieske-type clusters were later also found in bacterial dioxygenases [5]. The analysis of the EPR spectra of Rieske clusters has been a major challenge for modern advanced EPR techniques including electron nuclear double resonance (ENDOR) and electron spin echo envelope modulation (ESEEM) spectroscopy. From these studies in combination with mutational analyses, it was predicted that the [2Fe–2S] cluster should have two histidine ligands coordinating through their Nδ atoms to one iron atom (Fe^{2+} of the reduced cluster) [6–8].

A water soluble fragment containing the [2Fe–2S] cluster was first isolated from *Neurospora crassa* by Li *et al.* [9]. We have isolated a water soluble fragment (iron–sulfur fragment, ISF) of bovine heart mitochondrial bc_1 complex containing the intact [2Fe–2S] cluster. This fragment was found to be highly suited for electrochemical [10] and

spectroscopic [11–13] studies. It contains residues 68–196 of the mature iron–sulfur protein; its molecular weight including the [2Fe–2S] cluster is 14592 Da. Recently, we reported the crystallization of this fragment [12]. It was isolated and crystallized in the reduced state; it lacks its hydrophobic membrane anchor but still contains the native metal center, as judged from EPR and circular dichroism (CD) spectroscopy as well as from its redox potential. This potential was found to be within 10 mV of the value reported for the Rieske cluster in the bc_1 complex [12]. We have determined the crystal structure of the ISF using the multiwavelength anomalous dispersion (MAD) technique and refined it at 1.5 Å resolution. Here, we present the structure of the ISF and of the Rieske [2Fe–2S] cluster in atomic detail.

Results and discussion

Refined structure

The crystal structure of the soluble domain of the ISF was determined by the MAD technique and has been refined against diffraction data to 1.5 Å spacings (Table 1). The electron density was well defined (Fig. 1) so that we could construct the atomic model for the whole molecule except for the N-terminal residues 68 and 69. These may be disordered and/or partially absent due to the presence of a secondary protease cleavage site at position 70. Residues 70–72 and 188–190 are the only disordered parts of the structure, with average B values of backbone and side chain atoms exceeding 20 Å^2. All residues surrounding the metal centre have average B factors below 11 Å^2. The model contains 167 water molecules, three of which are buried (Wat4, Wat6, and Wat14). The estimated mean coordinate error is 0.16 Å based on the SIGMAA method [14].

Table 1

Model refinement.

Residue range	70–196
Number of non-hydrogen atoms	1169
Number of water molecules included	167
Resolution range (Å)	10–1.5
Average temperature factors (Å^2)	
Main-chain atoms	6.9
Side-chain atoms	7.8
Metal center atoms	7.0
Water molecules	20.4
R-factor ($F > 2\sigma(F)$;$F > 0$)*	0.187;0.192
Number of reflections	15165;15880
Free R-factor ($F > 2\sigma(F)$;$F > 0$)	0.211;0.214
Number of reflections	781;817
Rms deviations from ideal values	
Bond length (Å)	0.009
Bond angles (°)	1.5
Dihedral angles (°)	27.0
Improper torsion angles (°)	1.4
Ramachandran plot (non-Gly, non-Pro residues)	
Residues in most favoured regions (%)	90.6
Residues in additionally allowed regions (%)	9.4
Residues in generously allowed regions (%)	0
Residues in disallowed regions (%)	0
Other structural quality indicators	
Number of bad contacts	0
Omega angle deviation (°)	2.5
Zeta angle deviation (°)	1.7
Hydrogen-bond energy standard deviation (kcal mol^{-1})	0.8
Overall G-factor	+0.3

*R-factor=$\Sigma_h||F(h)_{obs}|-|F(h)_{calc}||/\Sigma_h|F(h)_{obs}|$.

Overall fold

The ISF is a flat spherical molecule with dimensions of 45×40×25 Å. The structure contains three layers of antiparallel β sheets (Figs 2,3). Sheet 1 is formed by the strands β9, β10 and β1; sheet 2 by strands β2, β3 and β4 and sheet 3 by strands β5–β8. The only α helix and a long loop are inserted between strands β3 and β4. This helix and loop have contact with sheets 2 and 3 mostly through salt bridges and hydrogen bonds (see below). The central sheet 2 contains longer strands than the other sheets and may be regarded as the 'spine' of the protein.

The three β sheets can be represented by two β sandwiches. One consists of sheets 1 and 2 and the other of sheets 2 and 3. Both β sandwiches, which share the central sheet 2, have hydrophobic cores. The metal-binding site is at the top (see Fig. 2) of the β sandwich formed by the sheets 2 and 3. The cluster-binding fold can be separated from the rest of the structure and forms a small domain-like structure of its own; the [2Fe–2S] cluster is at the tip of the fold.

The overall fold of the ISF shows no resemblance to any iron–sulfur protein reported so far. We have performed a search using the program DALI [15], which allows one to search systematically for homologous 3D structural motifs in the Brookhaven protein data bank (PDB), and could not find any similar structure. However, the structure around the metal cluster resembles that of the metal-binding loops of rubredoxin (see below).

Structure of the cluster-binding site

The [2Fe–2S] cluster is coordinated by two cysteine and two histidine residues (Fig. 4). The ligands coordinating the cluster originate from loops β4–β5 and β6–β7 (loops are named according to the secondary structure elements at each end). Each loop contributes one cysteine and one histidine residue: Cys139 and His141 of loop β4–β5, and Cys158 and His161 of loop β6–β7. His141 and His161 are ligands for Fe-2 whereas Cys139 and Cys158 are ligands for Fe-1; thus, the coordination pattern is 2+2 compared to the 3+1 pattern (Cys–X_4–Cys–X_2–Cys…Cys) observed in plant-type ferredoxins. A 2+2 pattern comprising four cysteine ligands has recently been observed in one of

Figure 1

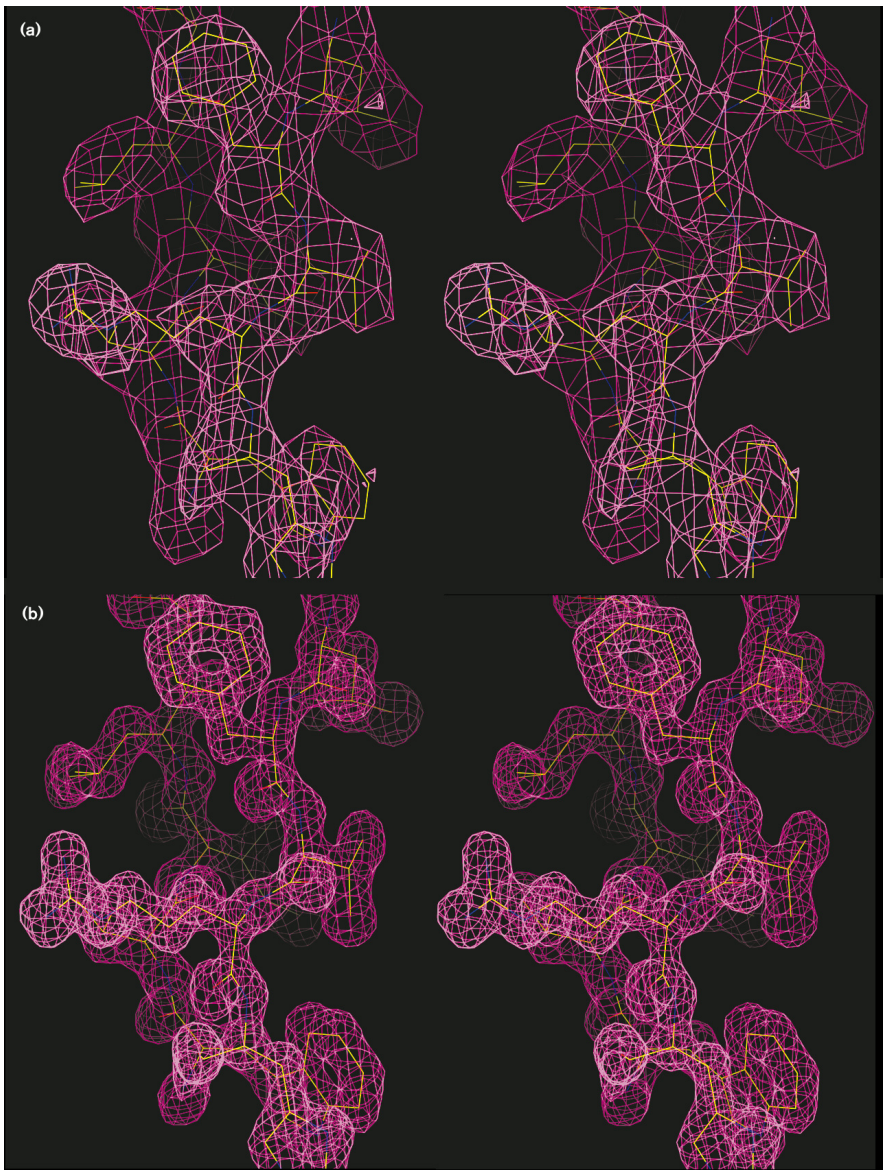

Representative part of the electron-density map of the iron–sulfur fragment (ISF) corresponding to parts of the strands β3 and β4. (a) Stereoview of the experimental electron-density map using the MAD phasing to 2.8 Å resolution shown superimposed on the refined model. (b) Stereoview of the SIGMAA-weighted [14] $2mF_o–DF_c$ electron-density map from the final model refined at 1.5 Å resolution shown superimposed on the refined model. Contour levels are 1.0 σ for the experimental map and 1.5 σ for the $2mF_o–DF_c$ map.

the [2Fe–2S] clusters of the molybdopterin-containing aldehyde oxidoreductase from *Desulfovibrio gigas* [16]; however, these structures again have no common features other than the coordination pattern.

Loops β4–β5 and β6–β7 both contain an additional cysteine residue (Cys144 and Cys160, respectively); these cysteines form a disulfide bond connecting the two loops (Fig. 3). The disulfide bond has left-handed chirality with a dihedral angle of –86.5°. The presence of this disulfide bond provides a rationale for the observation that mutation of each of the four (totally conserved) cysteine residues results in the loss of the cluster [17–19]; the disulfide bridge seems to be important for the stabilisation of the fold around the cluster as the two loops are not shielded by other parts of the protein. A third loop (residues 174–180, i.e. part of loop β8–β9) covers the cluster from the other side. Mutations in this 'Pro loop' containing the fully conserved sequence Gly–Pro175–Ala–Pro177 have shown that this loop is critical for cluster stability (see below).

The cluster-binding loops β4–β5 and β6–β7 show structural similarity to the metal-binding loops of rubredoxin. Rubredoxins are small (45–54 amino acids) electron transport proteins containing a single iron atom coordinated by four cysteine residues. The X-ray structures of four rubredoxins have been reported, the first being that of rubredoxin from *Desulfovibrio vulgaris* (RdDv) [20]. Figure 4c shows the superposition of the loops of the ISF and

Figure 2

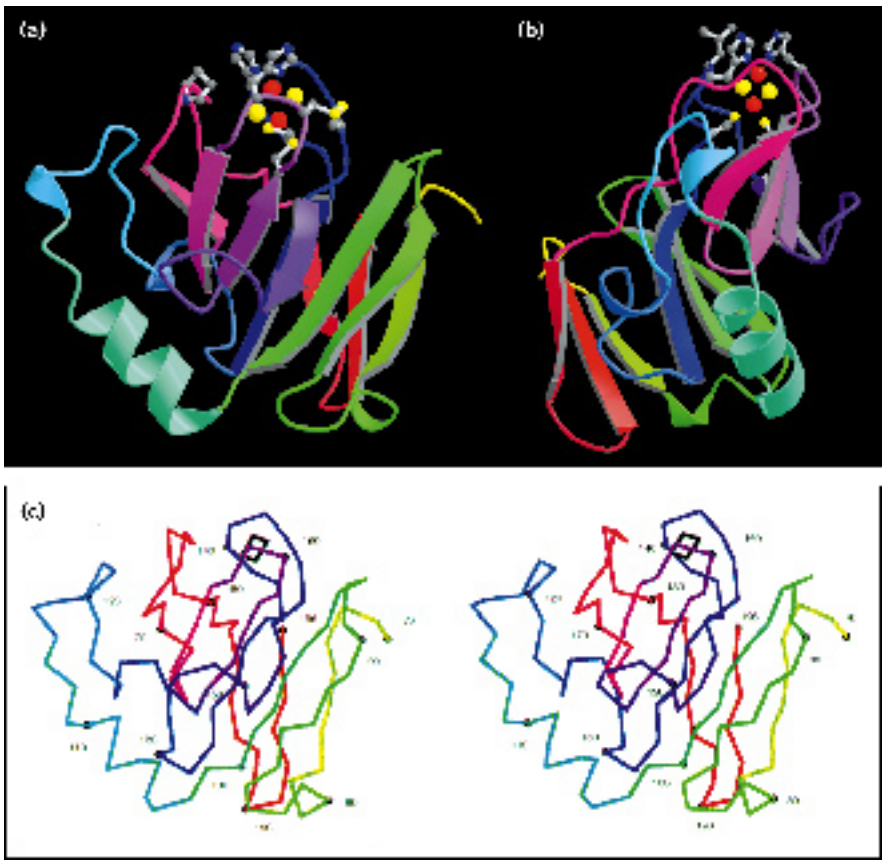

The structure of the ISF. (a) Schematic ribbon diagram showing atoms in the iron–sulfur cluster (red, iron; yellow, sulfur). The ligands of the cluster, the disulfide bond and residue Pro175 are also shown as ball-and-stick models. (b) View rotated by 90° showing Leu142 but not Pro175. The disulfide bridge is behind the [2Fe–2S] cluster and has been omitted for clarity. (c) Stereo drawing of the Cα backbone including residues 70–196, with coloring corresponding to that in (a),(b). Every tenth residue and the C-terminal residue have been numbered. The figures were produced using the programs MOLSCRIPT [48] and RASTER 3D [49].

oxidised RdDv (PDB accession number 7RXN) [21]. The root mean square (rms) deviation of the Cα atoms is 0.66 Å. However, both proteins show little structural homology except for the metal-binding loops, despite some similarity in their general topology; the sequence connecting the two metal-binding loops is much longer in all rubredoxins but there is no equivalent of the 'Pro loop'.

Comparison of the metal-binding loops of the ISF and RdDv shows that three out of the four residues coordinating the iron atoms are in equivalent positions in both proteins while the fourth cysteine of RdDv is in the position of Leu142 of ISF:

```
ISF  (138–144) VCTHLGC  (157–163) YCPCHGS
RdDv (5–11)    VCTVCGY  (38–44)   VCPLCGA
```

The two coordinating cysteine residues and iron atom Fe-1 of the ISF superpose with two of the coordinating cysteine residues (Cys6 and Cys39) and the iron atom of RdDv while the acid labile sulfur atoms of ISF superpose with the Sγ atoms of the other two cysteine residues of RdDv (Cys9 and Cys42). In addition, three non-coordinating residues of ISF (Gly143, Pro159, and Gly162) which are also present in RdDv are probably essential for the fold. RdDv does not contain a disulfide bridge connecting the two loops but the residues that replace these cysteines, Tyr11 and Leu41, are in van der Waals contact. This situation may resemble the structure in the Rieske-type ferredoxins from dioxygenases in which an aromatic residue (tryptophan) and leucine are found in these positions [5].

There is an interesting analogy between the Rieske protein of the bc_1 complex and subunit II of cytochrome oxidase. Both subunits have their redox centers in hydrophilic domains that are connected to the rest of the complex through N-terminal membrane anchors. Also, they both have dinuclear metal centers (the [2Fe–2S] center and the di-copper Cu_A center, respectively) and their protein structures show some similarity to mononuclear redox proteins (rubredoxin and plastocyanin, respectively) [22]. In both cases, one of the metal ions of the dinuclear center superposes on the metal ion of the respective mononuclear counterpart. Therefore, it seems that both subunits may have originated from the water soluble mononuclear redox proteins that were incorporated into the respective membrane protein complex. This would provide a rationale for the fact that the Rieske protein is not related to [2Fe–2S] ferredoxins.

Figure 3

Topology of the ISF. The hydrogen-bond pattern and secondary structure assignment are indicated. The residues conserved in all known Rieske iron–sulfur proteins from cytochrome bc_1 complexes are printed in red. The outlined characters denote residues missing in Rieske iron–sulfur protein from the cytochrome b_6f complex. Metal ligands and residues that form a disulfide bridge are colored yellow and green, respectively.

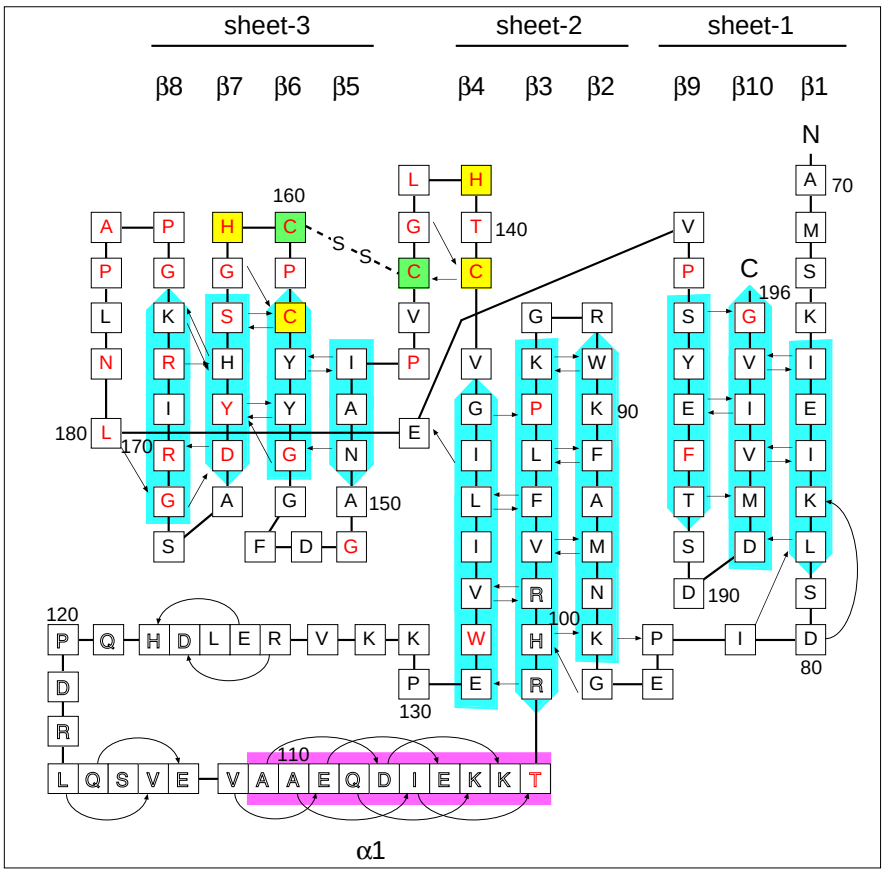

Structure of the [2Fe–2S] cluster

The distance between the two iron atoms is 2.7 Å; characteristic bond lengths and angles around the metal center are given in Table 2. The distances are compatible with those obtained from extended X-ray absorption fine structure (EXAFS) measurements [23,24]; however, we found the iron–nitrogen distance to be slightly greater (2.14 compared with 2.10 Å). The coordinating sulfur atoms form an almost perfect tetrahedron around Fe-1; the deviation of the S–(Fe-1)–S angles from the ideal value of 109.5° is less than ±5° (Table 2). In contrast, Fe-2 shows a marked reduction of the tetrahedral symmetry both by the presence of two histidine ligands as well as by a distortion of the coordination geometry; the Nδ–(Fe-2)–Nδ angle is 91°, a value expected for octahedral coordination. The two iron atoms, the Sγ atoms of both cysteine ligands and the Nδ atoms of the histidine ligands are nearly, but not exactly, in one plane; the planes defined by Sγ–(Fe-1)–Sγ and Nδ–(Fe-2)–Nδ are twisted by +8° around the axis defined by the Fe–Fe bond. The vector between the bridging sulfur atoms is perpendicular to the plane defined by Sγ–(Fe-1)–Sγ. This is as expected for the tetrahedral geometry of the Fe-1; the twist occurs around Fe-2. This chirality of the cluster provides a rationale for the intense CD spectra characteristic of all Rieske clusters [13,25,26].

The position of all sulfur atoms is tightly constrained by the presence of multiple hydrogen bonds (Table 2); all except one sulfur atom participate in two NH–S or OH–S hydrogen bonds in addition to the iron and carbon bonds. The exception is Sγ of Cys158, which has only a single hydrogen bond to the nitrogen atom of Cys160. This pattern contributes to the stability of the cluster. Nitrogen, oxygen and iron atoms around each sulfur atom form regular or distorted tetrahedrons. Hydrogen bonds between a cysteine Sγ atom of the ith residue and a main chain N atom of the $(i+2)$th residue are common features in iron–sulfur proteins. In the structure presented here, both Cys139 Sγ–His141 N and Cys158 Sγ–Cys160 N form type-I turns [27]. Two OH–S hydrogen bonds are observed: S-1–Ser163 Oγ and Cys139 Sγ– Tyr165 Oη. Both Ser163 and Tyr165 are conserved in all known bc_1 Rieske iron-sulfur proteins and should be important for the properties of the metal center; mutations in either residue led to a complete loss of the cluster [28,29].

The coordination environment of the Rieske clusters has previously been predicted from the analysis of ENDOR and ESEEM spectra [6–8]. However, the details of the model predicted [7] differ from the structure of the

Figure 4

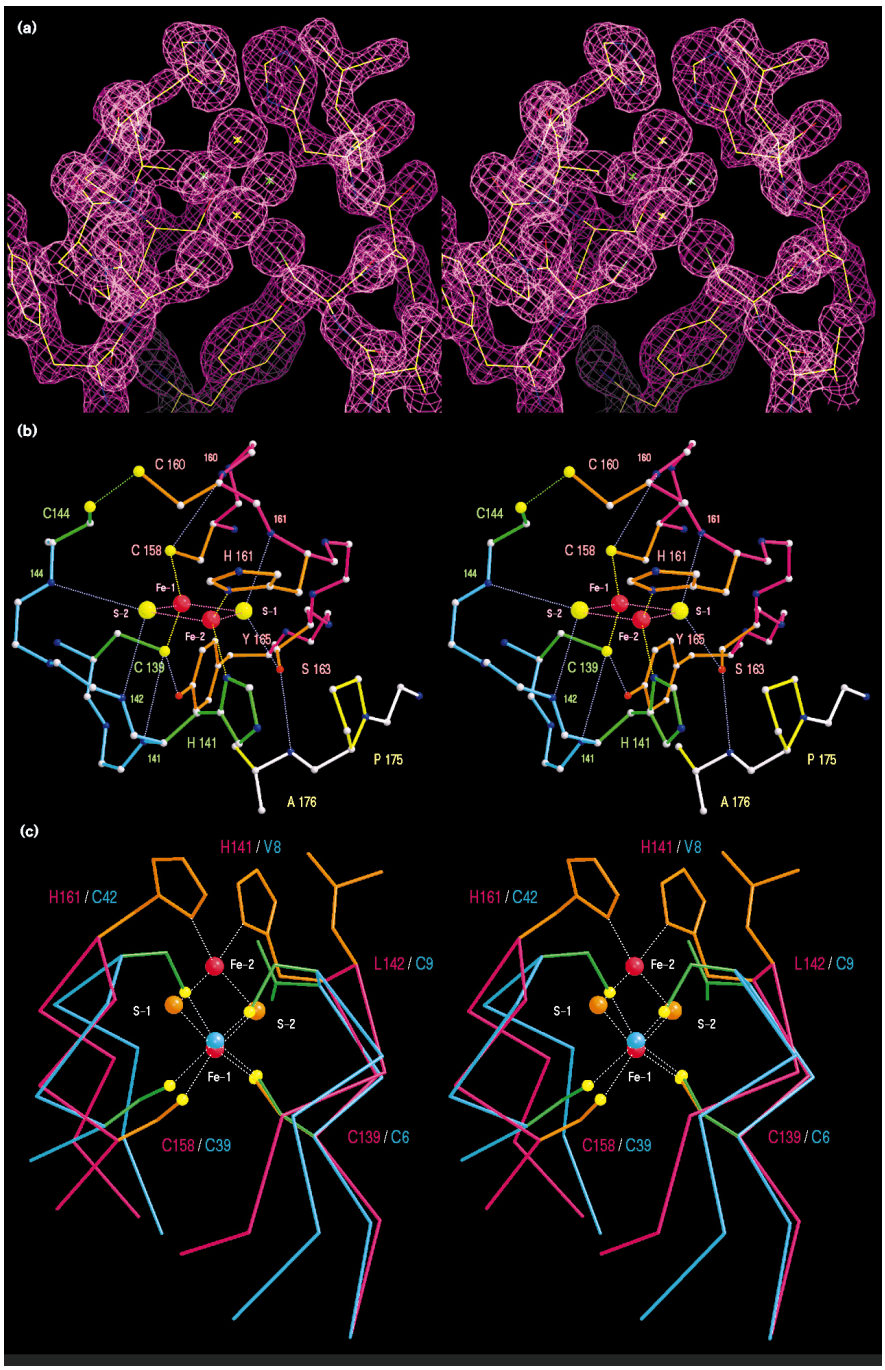

The structure of the Rieske iron–sulfur cluster. **(a)** Stereoview of the SIGMAA-weighted $2mF_o$-DF_c electron-density map of the iron–sulfur cluster at 1.5 Å (stereoview) and a contour level of 1.5σ. Sulfur atoms are indicated in green and the yellow crosses represent iron atoms. **(b)** Stereoview of the iron–sulfur cluster. Bonds within the [2Fe–2S] cluster are colored red; those between iron atoms and ligands are in yellow; the disulfide bridge is in green; and NH–S and OH–S hydrogen bonds are in blue. Standard colours are used for atoms. **(c)** Stereoview showing superposition of the metal-binding sites of the ISF (residues 137–146 and 157–165) and of RdDv [21] (residues 4–13 and 38–46). Cα traces and residue labels are magenta and cyan for the ISF and RdDv, respectively. Side chains involved in metal binding and those in equivalent positions are shown in orange and green, respectively. Inorganic sulfur atoms are represented as orange balls and iron atoms as red and cyan balls in ISF and RdDv, respectively.

reduced cluster presented here. The coordination of the histidine ligands to the Fe-2 is much more asymmetric than predicted from the analysis of the ENDOR spectra: the angles between the axes defined by the Fe–Fe bond and the Fe-2–Nδ vector are 52° and 39° for His141 and His161, respectively. The orientation of the His141 imidazole plane is close to that of the Nδ–(Fe-2)–Nδ plane (inclination 12°) whereas the imidazole of His161 is oriented perpendicularly to this plane (inclination 82°).

In the reduced cluster the additional electron is localised, that is, one iron has a formal charge of +2 and the other iron of +3. Möβbauer spectroscopy of a Rieske protein from *Thermus thermophilus* indicated that the iron in the Fe(II) state is that with nitrogen coordination (Fe-2) [25]; this is consistent with the consideration that the Fe(II) state is stabilized more by the neutral imidazole ligands than by two thiolate ligands. Both iron atoms and the sulfur atom S-1 have no solvent-accessible surface as determined by

Table 2

Important distances and angles at the metal center.

Fe–S	
Bond distances (Å)	
Fe-1–S	2.24/2.25
Fe-2–S	2.23/2.25
Fe-1–Fe-2	2.71
Bond angles (°)	
Fe–S–Fe (average)	74.4
S–Fe–S (average)	105.6
Fe ligands	
Bond distances (Å)	
Fe-1–Cys139 Sγ	2.29
Fe-1–Cys158 Sγ	2.22
Fe-2–His141 Nδ	2.16
Fe-2–His161 Nδ	2.13
Bond angles (°)	
Cys139 Sγ–Fe-1–Cys158 Sγ	105.6
His141 Nδ–Fe-2–His161 Nδ	90.8
NH–S and OH–S hydrogen bonds (Å)	
S-1–His161 N	3.24
S-1–Ser163 Oη	3.19
S-2–Leu142 N	3.15
S-2–Cys144 N	3.60
Cys139 Sγ–Tyr165 Oη	3.07
Cys139 Sγ–His141 N	3.53
Cys158 Sγ–Cys160 N	3.83

the program SURFACE of the CCP4 suite [30]. Fe(II) is close to the surface of the protein with its histidine ligands fully exposed to the solvent whereas Fe(III) (Fe-1) is buried within the protein and surrounded by the three loops forming the cluster-binding fold. Multiple factors contribute to the high redox potential of the cluster: the overall charge of the cluster, 0 and –1 for the oxidised and reduced state, respectively, compared with –2 and –3 for [2Fe–2S] clusters with four cysteine coordination; the electronegativity of the histidine ligands; and the solvent exposure of the Fe(II). The last factor was found to be largely responsible for the observed differences in redox potential between the Rieske center of the bc_1 complex presented here and the Rieske center in bacterial dioxygenases, which has a much more negative redox potential [13].

Salt bridge/hydrogen-bond network

The strands β7 and β8 contain several fully conserved charged residues (Asp166, Arg170 and Arg172). These residues are involved in an internal salt bridge/hydrogen-bond network (Fig. 5) that connects the bottom part of the cluster-binding fold (β6, β7, and β8) to the α1 helix, the α1–β4 loop, and the lower part of strand β3 (Fig. 5). Five arginine residues (Arg99, Arg101, Arg126, Arg170, and Arg172) and 4 acidic residues (Glu105, Glu109, Asp123, and Asp166) are involved in the network. We suggest that the complex salt bridge network is essential for the stability of the protein.

Glu109, Asp166, Arg170, and Arg172 form a complex salt bridge network; between Glu109 and Arg172 there is a bridging water molecule (Wat96). Asp166 and Arg170 are buried and form four and five salt bridges/hydrogen bonds to protein atoms, respectively. Arg172 and Glu109 are partially exposed and form hydrogen bonds to solvent molecules. Other residues are connected to this salt bridge network via hydrogen bonds, including residues Gln121, Arg126, Ala167 and Ser168 (Fig. 5b). Arg101 and Asp123 form a bifurcated salt bridge and they form additional hydrogen bonds to the carbonyl group of Ala167 and the Oγ of Ser168 as well as to the backbone carbonyl of Pro130. Through these interactions, the bottom of strand β3 is connected to helix α1, to the loop α1–β4, and to the cluster-binding fold. This structure is further stabilised by a salt bridge between Arg99 and Glu105, which is hydrogen bonded to the carbonyl groups of Gly154 and Gly155 in loop β5–β6 of the cluster-binding fold. The importance of the network is demonstrated by the fact that in a yeast mutant in which Asp166 had been replaced by asparagine, no [2Fe–2S] cluster could be observed [28].

Complex salt bridges have recently been observed in hyperthermostable proteins [31–33] and in these proteins, arginine is often found instead of lysine. This substitution is considered to be essential for thermostability as arginine can form up to five salt bridges/hydrogen bonds in different directions instead of the three bridges formed by lysine. The Rieske fragment is remarkably stable and is not attacked by proteases; this is probably due to the tight packing and to the fact that the loop regions are not flexible but fixed by the salt-bridge network.

Conserved residues and analysis of mutants

All but six conserved residues (Fig. 3) occur within the cluster-binding fold. These exceptions are the C-terminal residue Gly196; Pro95 and Pro183, which are located in loop regions; two aromatic residues (Trp132 and Phe187) in the lower part of the molecule (Fig. 2); and Thr102 at the beginning of the helix α1.

Using a random mutagenesis approach, respiratory deficient [28] and temperature-sensitive [29,34] mutants of the Rieske protein have been selected in yeast. These include mutations in the conserved residues Pro95, Trp132 and Pro183 and in residues in the Pro loop. The Trp132→Arg mutation had the most severe effect. Also, for mutants in which either of the aforementioned prolines was converted to serine or leucine the activity was less than 20% of the wild type. In the Pro175→Ser mutant this was due to the instability of the cluster; the specific activity per [2Fe–2S] cluster was not reduced [28]. The same result was found for the mutant Ala176→Thr [28], whereas the mutant Ala176→Val was inactive [29].

Mutations of conserved residues in the vicinity of the [2Fe–2S] cluster prevented its assembly; these included mutations in the four ligands, in the cysteine residues

Figure 5

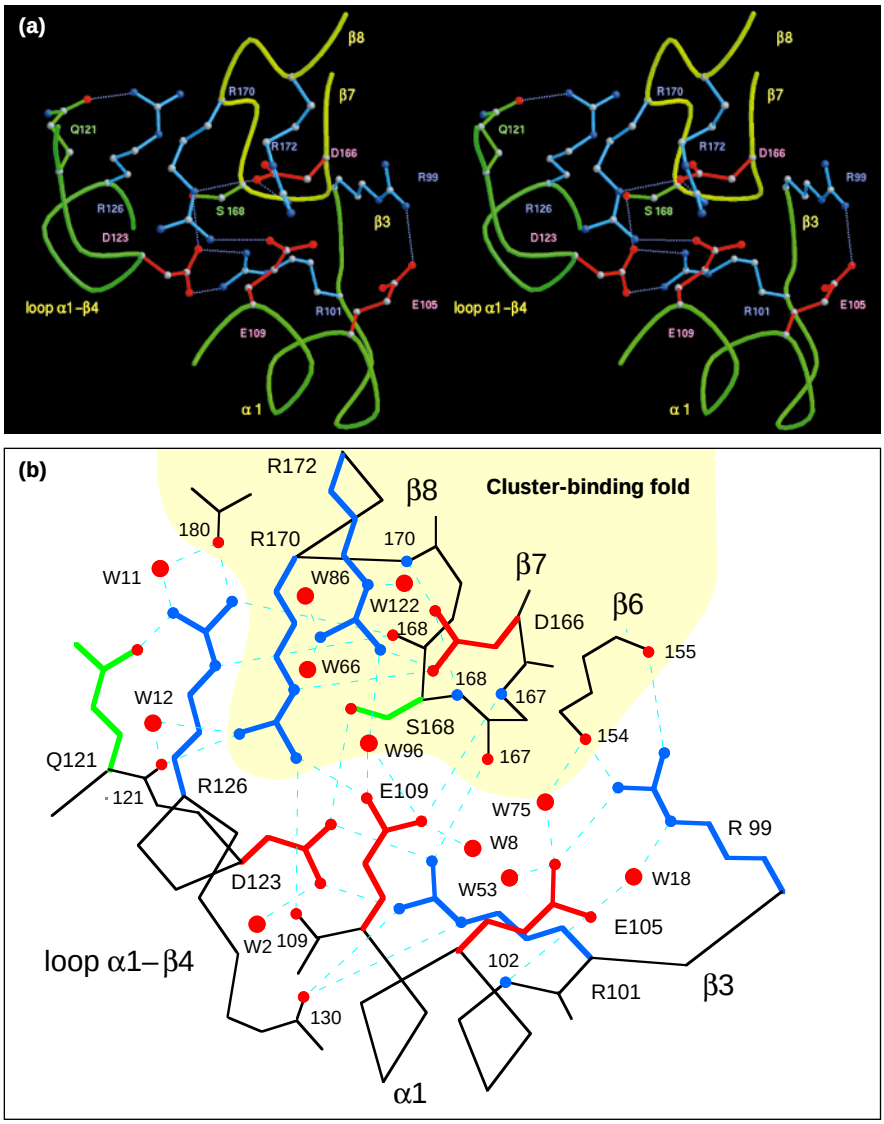

Salt bridge/hydrogen-bond network of the ISF. (a) Stereoview of a part of the salt bridge/hydrogen-bond network in the region connecting the bottom part of the cluster-binding fold to the lower parts of strand β3, the helix α1, and the loop α1–β4 (see text). Only interactions between side chains are shown. Standard atom coloring is used. (b) Schematic representation of essential salt bridges/hydrogen bonds within the network. Side chains are shown in color: acidic, red; basic, blue; neutral, green. The region comprising the metal-binding fold is in yellow.

forming the disulfide bridge, and in residues Tyr165 and Asp166 (see above).

Within strand β8 and the Pro loop, mutations leading to complete loss of activity were also found at positions 168 (Ser→Pro), 169 (Gly→Asp), 170 (Arg→Gly), and 179 (Asn→Lys) [29]. Other mutants in which the salt bridge network was affected showed 20–30% of the wild-type activity, probably due to instability of the protein. These included the mutants Glu105→Gly, Asp123→Asn, and Asp123→Gly [29].

Gatti *et al.* [28] have identified three mutants in which the midpoint potential (E_m) of the [2Fe–2S] cluster was altered: Gly143→Asp ($\Delta E_m = -96$ mV), Pro146→Leu ($\Delta E_m = -98$ mV), and Pro159→Leu ($\Delta E_m = -53$ mV). Two of these positions are adjacent to the disulfide bridge (143,159). Gly143 has φ and ψ angles of 91° and 2°, respectively; these values are outside the favourable region for non-glycine residues therefore the Gly143 mutation should cause conformational changes. Pro146 is in a unique position in which the backbone is folded 'inwards' immediately preceding strand β5. The side chain of a leucine in this position would be within van der Waals distance of both Tyr165 and Cys158 therefore a conformational change must also occur in the mutant Pro146→Leu. Mutation of the exposed Pro159 will increase the flexibility of the cluster-binding loop. Thus, all three mutations will lead to a distortion of the protein environment of the [2Fe–2S] cluster and most probably of the hydrogen-bonding network surrounding the cluster (see above) and will thus influence the redox potential.

The three mutations are all in a part of the fold that is stabilised through the presence of the disulfide bond and they retain the cluster 30–68% of the time [28]. This is in contrast to the mutations in the strand β8 and in the Pro loop which lead largely to the loss of the cluster.

Using site-directed mutagenesis in *Rhodobacter capsulatus*, Liebl *et al.* [35] have converted the conserved Thr140 (Thr134 in *Rb. capsulatus*) into glycine, aspartate, histidine and arginine. Thr140 is packed against the Pro loop; the Oγ forms a hydrogen bond with the backbone nitrogen of Leu178. The mutation Thr140→Asp destroyed the cluster and all other mutations led to a perturbation of the cluster, with lowered redox potentials and increased oxygen sensitivity [35]. This again demonstrates the importance of the packing of the Pro loop.

Charge distribution of the protein surface

Figure 6 shows the surface electrostatic potential of ISF. The tip of the protein that surrounds the metal cluster has a non-polar surface whereas the bottom (see Figs 2,6) is polar. The surface surrounding the base of the protein is predominantly acidic whereas β sheet 2 and the surface of the strand β8 are predominantly basic. The helix α1 and the loop α1–β4 contain in total six acidic and six basic residues which make this region, together with the bottom parts of sheets 2 and 3, the most polar part of the protein.

The hydrophobic surface around His141 and His161 is likely to form part of the Q_P quinone-binding site of the bc_1 complex. This is located at the interface between the Rieske protein and cytochrome *b*, within or close to the membrane (see below). The position of the N terminus of the fragment, which is connected to the membrane anchor in the full Rieske protein, supports this idea.

The only highly conserved parts of ISF that are neither involved in metal binding nor essential for the fold (see above) are the bottom parts of the cluster-binding fold (Figs 2,3). As we would expect the interface between the Rieske protein and cytochrome c_1 to be conserved, we suggest that this part of the cluster-binding fold may be involved in this interaction. This assignment is supported by a comparison between the Rieske proteins from bc_1 and b_6f complexes; both cytochrome *b* and the Rieske protein are highly conserved whereas cytochrome c_1 and cytochrome *f* are functionally equivalent but show no detectable sequence homology except for the heme- binding pentapeptide. So far, only the structure of the water soluble domain of cytochrome *f*, but not cytochrome c_1, has been determined [36]. The helix α1 and the loop α1–β4, which are adjacent to the proposed site for interaction with cytochrome c_1, are missing in the Rieske protein from b_6f complexes (Fig. 3). Therefore, structural differences between cytochrome c_1 and cytochrome *f* are likely to be related to structural differences in the interaction region on ISF.

Figure 6

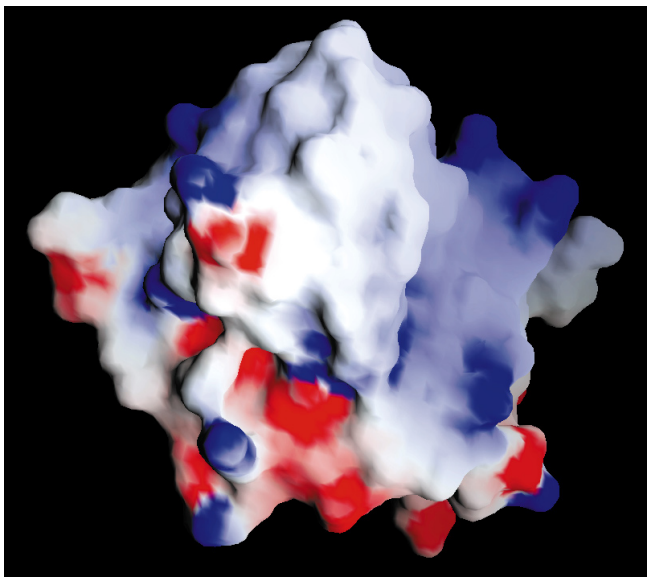

Electrostatic surface properties of the ISF. Molecular surface of ISF color-coded by electrostatic potential: red, negative; blue, positive. The extreme ranges of red and blue represent electrostatic potentials of –5 and +5 k_BT, respectively (k_B, Boltzmann constant; T, temperature). The view shows the same orientation as Figure 2a. The figure was generated using the program GRASP [50].

Functional significance of the Rieske cluster in the Q_P pocket

The Rieske [2Fe–2S] protein is the first electron acceptor during the oxidation of hydroquinone. It is also the primary binding site for two classes of inhibitors, the chromone inhibitor stigmatellin and hydroxyquinones which show strong structural homology to the natural substrate, ubiquinone [37]. The affinity of the bc_1 complex for stigmatellin is largely decreased when the iron–sulfur protein is depleted [38]; stigmatellin binds five orders of magnitude more tightly to the reduced than the oxidised [2Fe–2S] cluster and shifts the high-field g-value (g_x) signal of the EPR spectrum [39]. Stigmatellin also binds in the secondary quinone-binding (Q_B) site of the photosynthetic reaction center from purple bacteria. It binds in the same position as ubiquinone via a hydrogen bond to residue HisL190 which is a ligand to the Fe^{2+} [40]. In the structure presented here, the Nε atoms of both histidine ligands to Fe-2 (Fe(II) in the reduced cluster) are completely exposed to solvent within a hydrophobic surface at the tip of the structure (Fig. 2); Leu142 is exposed at the hydrophobic tip adjacent to the histidine ligands. In *Rb. capsulatus*, mutation of this residue (Leu136 in *Rb. capsulatus*) to glycine, asparagine, histidine or arginine completely blocked quinone binding although the structure and the redox potential were apparently unperturbed [35]. All these data indicate that the histidine ligands are part of the binding site for both stigmatellin and quinones in the Q_P pocket of the bc_1 complex. However, neither inhibitors

nor substrates will bind to the isolated ISF (TA Link, unpublished results) indicating that other parts of the bc_1 complex, probably cytochrome *b*, form the major part of the quinone-binding site.

The redox potential of the isolated ISF is the same, within 10 mV, to that of the Rieske cluster in the bc_1 complex [12]. From this, we conclude that the polarity within the Q_P pocket is high. In the photosynthetic reaction center from purple bacteria, the Q_B site is filled with six ordered water molecules when quinones are not present [40].

The redox potential of the Rieske [2Fe–2S] cluster is pH dependent; from the pH dependence, two groups with redox dependent pK values could be determined [10]. The pK values of 7.6 and 9.2 of the oxidised protein shift to above 11 in the reduced protein. The deprotonation of the oxidised protein could also be observed in the CD spectrum of the [2Fe–2S] cluster, indicating that this is not a general electrostatic effect. From these data, it has been proposed that deprotonation should occur on the histidine ligands of the Rieske cluster [11]. This proposal is strongly supported by the structure of ISF. The hydrogens at the Nϵ atoms of the histidine ligands are fully exposed and are not involved in any hydrogen bond. In addition, there are no other residues in the vicinity of the cluster that are likely to undergo redox dependent protonation/deprotonation. The fully conserved Tyr165 is not exposed to solvent and the Oη is hydrogen bonded to the Sγ of Cys139 (see above).

Biological implications

Iron–sulfur proteins are ubiquitous and they are thought to have been among the first metalloproteins to have arisen during the evolution of living cells. In most of the iron–sulfur proteins known, the iron atoms are coordinated by thiolates of cysteine residues. This work provides the first structure of an iron–sulfur protein containing a Rieske–type [2Fe–2S] cluster which involves two imidazole ligands. Rieske–type clusters have been found in archaebacteria, eubacteria, and eukaroytes; they form part of hydroquinone oxidising cytochrome *bc* (bc_1 or b_6f) complexes in respiratory and photosynthetic electron transport chains. They transfer one electron from the donor hydroquinone to cytochrome c_1 or *f*; from there, the electron goes to the acceptor, that is, cytochrome *c* or plastocyanin. Thus, the Rieske protein and cytochrome c_1/f form the 'high-potential' electron transfer chain at the positive-side (P-side) of the membrane within the *bc* complexes.

The imidazole ligands are instrumental in maintaining the high redox potential of the Rieske cluster; another factor contributing to the redox properties is the surface exposure of both imidazole rings. As the cluster is exposed at the tip of the structure, it can come into contact with the electron donor hydroquinone when the quinone is bound to cytochrome *b* within the hydroquinone oxidation pocket (Q_P). Due to the redox dependence of the pK values of the histidine ligands of the Rieske cluster, these histidines will take up protons upon reduction. This reaction may be essential for hydroquinone oxidation in the Q_P pocket; the availability of the structure of the Rieske center will allow the design of specific mutants that can be used to probe the reaction sequence during hydroquinone oxidation.

Another important feature of the protein is its high stability. This is maintained both through a strong salt bridge/hydrogen-bonding network as well as through the presence of a disulfide bridge. The presence of a disulfide bond is a rare feature in iron–sulfur proteins and the occurrence of a fully exposed disulfide bond next to the iron–sulfur cluster is unprecedented. The presence of the disulfide bond has important implications with regard to the sequence of the steps leading to the folding and assembly of the cluster within the bc_1 complex. In eukaryotes, the Rieske protein is synthesised with a presequence in the cytosol and must be imported into the mitochondria. Cleavage of the presequence occurs when the protein is already incorporated in the bc_1 complex [29]. At which stage and by which reactions the [2Fe–2S] cluster is incorporated and disulfide bridge is formed, remain to be elucidated.

Materials and methods

Crystallization

The proteolytic fragment and crystals were prepared as described in [12]. The crystallisation of the ISF was performed at pH 6.2 with 23% PEG 6000 using the hanging drop technique in nitrogen atmosphere.

Data collection and characterization of the ISF crystals

The crystals belong to the monoclinic space group $P2_1$. The cell dimensions of the crystals are: a=32.1 Å, b=53.0 Å, c=38.0 Å and β=100.3° (based on the data set measured at 100 K). The asymmetric unit contains one ISF molecule. The solvent content is 41%.

Data for MAD phasing were collected at three different wavelengths using the Weissenberg camera system for macromolecules [41] at the beamline BL18B of the Photon Factory (Tsukuba, Japan). The X-ray fluorescence spectrum of the ISF near the K-shell edge of iron was measured initially. This was used to select monochromator settings for the peak (1.738 Å, maximum of f″), the inflection point (1.760 Å, minimum of f′) and one remote point (1.800 Å). Due to technical problems, we could not measure the data at 1.000 Å at the same time as planned originally but the data were collected at beam line BL6A2 at the Photon Factory. The crystals were precisely aligned such that Bijvoet pairs could be recorded simultaneously. The data collection at BL18B was done with one frozen crystal at the three wavelengths at 100 K. This minimized systematic errors and scaling between three data sets was then straightforward. The Weissenberg images were read out with a Fuji BAS2000 scanner. These images were processed and scaled by programs DENZO and Scalepack [42]. The data collection is summarized in Table 3.

Structure determination using MAD phasing

Data at three different wavelengths (1.800, 1.760, and 1.738 Å) were scaled to data measured at 1.000 Å by program SCALEIT of the CCP4 program suit [30]. The heavy atom positions were determined

Table 3

Data collection.

Data set	Resolution range (Å)	Number of observations	Number of unique reflections	Completeness (%)*	Number of Bijvoet pairs	R_{merge} (%)†	R_{disp} (%)‡
1.800 (Remote λ1)	40.0–2.8	6835	2636	83.6 (63.8)	–	2.6 (3.1)	–
1.760 (Inflection λ2)	40.0–2.8	7985	2907	88.5 (71.4)	2 221	3.3 (4.0)	1.6 (3.0)
1.738 (Peak λ3)	40.0–2.8	7246	2715	84.9 (65.4)	2 038	3.8 (4.5)	2.7 (3.8)
1.000 (Remote λ4)	40.0–1.5	63 633	18 058	89.4 (68.0)	–	5.1 (27.0)	6.4 (7.3)

* Numbers in the brackets are for the last shells. †$R_{merge}=\Sigma_h\Sigma_i|I_i(h)-<I(h)>|/\Sigma_h\Sigma_i I_i(h)$ where $I_i(h)$ is the ith measurement. ‡$R_{disp}=\Sigma||F_p(\lambda_a)|-|F_p(1.800)||/\Sigma|F_p(1.800)|$, where $F_p(\lambda_a)$ and $F_p(1.800)$ are protein structure factors at λ_a (1.760, 1.738 or 1.000) and 1.800 Å, respectively.

using difference Patterson maps. In the Harker sections of anomalous difference Patterson maps (at 1.760 and 1.738 Å) and a dispersive difference Patterson map ($||F(1.760)|-|F(1.800)||^2$), the positions of the two iron atoms of the metal center were clearly observed. From these peak positions and the known distance between two iron atoms (2.7 Å) determined by EXAFS [23,24], we could obtain initial positions for the two iron atoms.

Phase refinement of these iron positions and MAD phasing were performed using program MLPHARE [43]. For the phasing using MLPHARE, the data at 1.800 Å were assumed to be the native set and the other two to be the derivatives. The primary phases were calculated using the data in the range from 30.0 and 2.8 Å resolution. Then, density modification (solvent flattening and histogram mapping) using the program DM [44] was performed and as a result the free-R factor dropped from 0.559 to 0.270. In the electron-density map we could trace most of the main chain of the protein but the density for side chains was poor. We performed phase refinement and MAD phasing again with the program MLPHARE, using the improved phases after the density modification. From the statistics of phasing (Table 4), it is clear that the MAD phases were well estimated up to 4 Å resolution but those for higher resolution data were rather poor due to several experimental limitations now described. The data set at λ=1.000 Å was collected from a different crystal and at a different beam line from the other three data sets; this data set could not be used for phasing as the scaling error was relatively large. Also, due to limitations imposed by the size of the imaging plate, we could collect data at λ=1.800, 1.760, and 1.738 Å along the rotation axis only up to 4.3 Å resolution.

In order to improve the phases, further density modification using the program SOLOMON was applied [45]. The best result was obtained from twelve cycles of SOLOMON run at 4.0 Å without solvent flipping, followed by 72 phase extension cycles from 4.0 Å to 2.8 Å with a flipping factor of –0.7 and 18 more cycles at 2.8 Å with the same flipping factor. The R-factor dropped from 0.533 to 0.064. The first 12 cycles at 4.0 Å without flipping were essential in order to get a high quality map as the density modification using solvent flipping has a large convergence radius but is sensitive to the initial map quality. The final modified density map was sufficient for model building (Fig. 1).

Model building and refinement

The atomic model was constructed using program O [46]. The R-factor (to 3 769 reflections in the range from 6 to 2.8 Å resolution) and the free-R factor (to randomly selected 194 reflections in the same range) for the initial model including 124 amino acid residues (residues 73–196) were 0.45 and 0.46, respectively. These were reduced to 0.26 (R-factor) and 0.40 (free-R factor), respectively, in one round of simulated annealing with X-PLOR [47]. The model was finally refined at 1.5 Å resolution. The model includes 127 amino acids (residues 70–196), two iron and two sulfur atoms and 167 water molecules. The final R-factor (to 15 165 reflections in the range from 10 to 1.5 Å resolution) and free-R factor (to 781 reflections in the same range) were 0.187 and 0.211, respectively. As the diffraction from the crystals showed anisotropic resolution, an overall anisotropic B-factor was applied. The anisotropic B-factor tensor is expressed as $B_{11}=-6.5$, $B_{22}=0.52$, $B_{33}=6.0$, $B_{12}=0.0$, $B_{13}=-3.2$ and $B_{23}=0.0$. The refinement and the quality of the final model are summarized in Table 1.

Accession numbers

The final coordinates and the structure factors have been deposited with the Protein Data Bank (accession number 1RIE).

Table 4

Phase calculation using MLPHARE.

Data set	Fe-1		Fe-2		R_{cullis}‡	R_{cullis_ano}§	Phasing power at each resolution bin (Å)								
	Occ*	Aocc†	Occ*	Aocc†			(14.1)	(8.8)	(6.5)	(5.1)	(4.2)	(3.6)	(3.2)	(2.8)	Total
1.760 (Inflection λ2)	–0.183	0.799	–0.170	0.730	0.61	0.78	1.47	2.09	2.59	1.88	1.62	0.77	0.55	0.58	0.61
1.738 (Peak λ3)	–0.128	1.023	–0.112	0.980	0.73	0.74	1.20	2.04	2.37	1.64	1.28	0.67	0.44	0.45	0.73
Figure of Merit							0.84	0.75	0.74	0.60	0.53	0.46	0.27	0.29	0.48

*Occupancy. †Anomalous occupancy. ‡$R_{cullis}=\Sigma|||F_p(\lambda_a)|-|F_p(1.800)||-|\Delta F_{calc}||/\Sigma||F_p(\lambda_a)|-|F_p(1.800)||$, where $F_p(\lambda_a)$ and $F_p(1.800)$ are protein structure factors at λ_a (1.760 or 1.738) and 1.800 Å, respectively. ΔF_{calc} is the calculated dispersive difference between at λ_a and 1.800 Å. Summation was done using centric reflections only. §$R_{cullis\_ano}=\Sigma|||F_p^+(\lambda_a)|-|F_p^-(\lambda_a)||-|\Delta F_{calc}||/\Sigma||F_p^+(\lambda_a)|-|F_p^-(\lambda_a)||$, in which $|F_p^+(\lambda_a)|-|F_p^-(\lambda_a)|$ is the Bijvoet difference at λ_a (1.760 or 1.738). ΔF_{calc} is calculated anomalous difference at λ_a.

Acknowledgements

We thank Drs N Sakabe, A Nakagawa and N Watanabe for many helpful suggestions during the MAD experiments in the Photon Factory, Tsukuba, Japan, and H Müller for technical assistance. The experiments using synchrotron radiation were performed under the approval of the Photon Factory Advisory Committee (Proposal No. 94G-035), National Laboratory for High Energy Physics, Japan. HM and SI are members of the TARA project of Tsukuba University, Japan. The crystallization project was funded by a grant to TAL from the Deutsche Forschungsgemeinschaft (DFG), Priority Programme 'Transition Metals in Biology and their Coordination Chemistry' (grant Li 474/2). We particularly thank one of the referees for drawing our attention to the structural homology between the metal-binding loops of the ISF and rubredoxin.

References

1. Rieske, J.S., Maclennan, D.H. & Coleman, R. (1964). Isolation and properties of an iron-protein from the (reduced coenzyme Q)–cytochrome c reductase complex of the respiratory chain. *Biochem. Biophys. Res. Commun.* **15**, 338–344.
2. Trumpower, B.L. & Edwards, C.A. (1979). Identification of oxidation factor as a reconstitutively active form of the iron-sulfur protein of the cytochrome *b*-c_1 segment of the respiratory chain. *FEBS Lett.* **100**, 13–16.
3. Trumpower, B.L. & Edwards, C.A. (1979). Purification of a reconstitutively active iron-sulfur protein (oxidation factor) from succinate·cytochrome *c* reductase complex of bovine heart mitochondria. *J. Biol. Chem.* **254**, 8697–8706.
4. Trumpower, B.L. (1981). Function of the iron-sulfur protein of the cytochrome *b*-c_1 segment in electron-transfer and energy-conserving reactions of the mitochondrial respiratory chain. *Biochim. Biophys. Acta* **639**, 129–155.
5. Mason, J.R. & Cammack, R. (1992). The electron-transport proteins of hydroxylating bacterial dioxygenases. *Annu. Rev. Microbiol.* **46**, 277–305.
6. Gurbiel, R.J., *et al*., & Ballou, D.P. (1989). Electron-nuclear double resonance spectroscopy of ^{15}N-enriched phthalate dioxygenase from *Pseudomonas cepacia* proves that two histidines are coordinated to the [2Fe–2S] Rieske-type clusters. *Biochemistry* **28**, 4861–4871.
7. Gurbiel, R.J., Ohnishi, T., Robertson, D., Daldal, F. & Hoffman B.M. (1991). Q-Band ENDOR spectra of the Rieske protein from *Rhodobacter capsulatus* ubiquinol-cytochrome *c* oxidoreductase show two histidines coordinated to the [2Fe–2S] cluster. *Biochemistry* **30**, 11579–11584.
8. Britt, R.D., *et al*., & Malkin, R. (1991). Electron spin echo envelope modulation spectroscopy supports the suggested coordination of two histidine ligands to the Rieske Fe-S centers of the cytochrome b_6f complex of spinach and the cytochrome bc_1 complexes of *Rhodospirillum rubrum, Rhodobacter sphaeroides* R-26, and bovine heart mitochondria. *Biochemistry* **30**, 1892–1901.
9. Li, Y., de Vries, S., Leonard, K. & Weiss, H. (1981). Topography of the iron-sulphur subunit in mitochondrial ubiquinol:cytochrome c reductase. *FEBS Lett.* **135**, 277–280.
10. Link, T.A., Hagen, W.R., Pierik, A.J., Assmann, C. & von Jagow, G. (1992). Determination of the redox properties of the Rieske [2Fe–2S] cluster of bovine heart bc_1 complex by direct electrochemistry of a water-soluble fragment. *Eur. J. Biochem.* **208**, 685–691.
11. Link, T.A. (1994). Two pK values of the oxidised 'Rieske' [2Fe-2S] cluster observed by CD spectroscopy. *Biochim. Biophys. Acta* **1185**, 81–84.
12. Link, T.A., Saynovits, M., Assmann, C., Iwata, S., Ohnishi, T. & von Jagow, G. (1996). Isolation, characterisation, and crystallisation of a water-soluble fragment of the Rieske iron-sulfur protein of bovine heart mitochondrial bc_1 complex. *Eur. J. Biochem.* **237**, 71–75.
13. Link, T.A., Hatzfeld, O.M., Unalkat, P., Shergill, J.K., Cammack, R. & Mason, J.R. (1996). Comparison of the Rieske 2-iron-2-sulfur centre in bc_1 complex and in bacterial dioxygenases by CD spectroscopy and cyclic voltammetry. *Biochemistry,* in press.
14. Read. R.J. (1986). Improved Fourier coefficient for maps using phases from partial structures with errors. *Acta Cryst.* A **42**, 140–149.
15. Holm, L. & Sander, C. (1993). Protein structure comparison by alignment of distance matrices. *J. Mol. Biol.* **233**, 123–138.
16. Romão, M.J., *et al*., & Huber, R. (1995). Crystal structure of the xanthine oxidase-related aldehyde oxido-reductase from *D. gigas*. *Science* **270**, 1170–1176.
17. Graham, L.A. & Trumpower, B.L. (1991). Mutational analysis of the mitochondrial Rieske iron-sulfur protein of *Saccharomyces cerevisiae*. III. Import, protease processing, and assembly into the cytochrome bc_1 complex of iron-sulfur protein lacking the iron-sulfur cluster. *J. Biol. Chem.* **266**, 22485–22492.
18. Davidson, E., Ohinshi, T., Atta-Asafo-Adjei, E. & Daldal, F. (1992). Potential ligands to the [2Fe–2S] Rieske cluster of the cytochrome bc_1 complex of Rhodobacter capsulatus probed by site-directed mutagenesis. *Biochemistry* **31**, 3342–3351.
19. Van Doren, S.R., Gennis, R.B., Barquera, B. & Crofts, A.R. (1993). Site-directed mutations of conserved residues of the Rieske iron-sulfur subunit of the cytochrome bc_1 complex of *Rhodobacter sphaeroides* blocking or impairing quinol oxidation. *Biochemistry* **32**, 8083–8091.
20. Herriott, J.R., Sieker, L.C., Jensen, L.H. & Lovenberg, W. (1970). Structure of rubredoxin: an X-ray study to 2.5 Å resolution. *J. Mol. Biol.* **50**, 391–406.
21. Adman, E.T., Sieker, L.C. & Jensen, L.H. (1991). Structure of rubredoxin from *Desulfovibrio vulgaris* at 1.5 Å resolution. *J. Mol. Biol.* **217**, 337–352.
22. Iwata, S., Ostermeier, C., Ludwig, B. & Michel, H. (1995). Structure at 2.8 Å resolution of cytochrome *c* oxidase from *Paracoccus denitrificans*. *Nature* **376**, 660–669.
23. Powers, L., Schägger, H., von Jagow, G., Smith, J., Chance, B. & Ohnishi, T. (1989). EXAFS studies of the isolated bovine heart Rieske [2Fe–2S]$^{1+(1+,2+)}$ cluster. *Biochim. Biophys. Acta* **975**, 293–298.
24. Tsang, H.-T., Batie, C.J., Ballou, D.P. & Penner-Hahn, J.E. (1989). X-ray absorption spectroscopy of the [2Fe–2S] Rieske cluster in *Pseudomonas cepacia* phthalate dioxygenase. Determination of core dimensions and iron ligation. *Biochemistry* **28**, 7233–7240.
25. Fee, J.A., *et al*., & Münck, E. (1984). Purification and characterization of the Rieske iron-sulfur protein from *Thermus thermophilus*. Evidence for a [2Fe–2S] cluster having non-cysteine ligands. *J. Biol. Chem.* **259**, 124–133.
26. Degli Esposti, M., Ballester, F., Solaini, G. & Lenaz, G. (1987). The circular-dichroic properties of the 'Rieske' iron-sulphur protein in the mitochondrial ubiquinol:cytochrome c reductase. *Biochem. J.* **241**, 285–290.
27. Adman, E., Watenpaugh, K. D. & Jensen, L. H. (1975). NH-S hydrogen bonds in *Peptococcus aerogenes* ferredoxin, *Clostridium pasteurianum* rubredoxin, and *Chromatium* high potential iron protein. *Proc. Natl. Acad. Sci. USA* **72**, 4854–4858.
28. Gatti, D.L., Meinhardt, S.W., Ohnishi, T. & Tzagoloff, A. (1989). Structure and function of the mitochondrial bc_1 complex. A mutational analysis of the yeast Rieske iron-sulfur protein. *J. Mol. Biol.* **205**, 421–435.
29. Graham, L.A., Brandt, U., Sargent, J.S. & Trumpower, B.L. (1992). Mutational analysis of assembly and function of the iron-sulfur protein of the cytochrome bc_1 complex in *Saccharomyces cerevisiae*. *J. Bioenerg. Biomembr.* **25**, 245–257.
30. Collaborative Computational Project Number 4 (1994). The CCP4 suite: programs for protein crystallography. *Acta Cryst.* D **50**, 760–763.
31. Musafia, B., Buchner, V. & Arad, D. (1995). Complex salt bridges in proteins: statistical analysis of structure and function. *J. Mol. Biol.* **254**, 761–770.
32. Yip, K.S.P., *et al*., & Rice D.W. (1995). The structure of *Pyrococcus furiosus* glutamate dehydrogenase reveals a key role for ion-pair networks in maintaining enzyme stability at extreme temperatures. *Structure* **3**, 1147–1158.
33. Hennig, M., Darimont, B., Sterner, R., Kirschner, K. & Jansonius, J.N. (1995). 2.0 Å structure of indole-3-glycerophosphate synthase from the hyperthermophile *Sulfolobus solfataricus*: possible determinants of protein stability. *Structure* **3**, 1295–1306.
34. Beckmann, J.D., Ljungdahl, P.O. & Trumpower, B.L. (1989). Mutational analysis of the mitochondrial Rieske iron-sulfur protein of *Saccharomyces cerevisiae*. I. Construction of a RIP1 deletion strain and isolation of temperature-sensitive mutants. *J. Biol. Chem.* **264**, 3713–3722.
35. Liebl, U., Sled, V., Ohnishi, T. & Daldal, F. (1995). Conserved non liganding residues of *Rhodobacter (R.) capsulatus* 'Rieske' protein are essential for [2Fe–2S] cluster properties and communication with the quinone pool. In *Photosynthesis: from Light to Biosphere*, Vol. II (Mathis, P., ed), pp. 749–752, Kluwer Academic Publishers, Dordrecht.
36. Martinez, S.E., Huang, D., Szczepaniak, A., Cramer, W.A. & Smith, J.L. (1994). Crystal structure of chloroplast cytochrome f reveals a novel cytochrome fold and unexpected heme ligation. *Structure* **2**, 95–105.
37. von Jagow, G. & Link, T.A. (1986). Use of specific inhibitors on the mitochondrial bc_1 complex. *Methods Enzymol.* **126**, 253–271.
38. Brandt, U., Haase, U., Schägger, H. & von Jagow, G. (1991). Significance of the 'Rieske' iron-sulfur protein for formation and function of the ubiquinol oxidation pocket of mitochondrial cytochrome *c* reductase (bc_1 complex). *J. Biol. Chem.* **266**, 19958–19964.

39. von Jagow, G. & Ohnishi, T. (1985). The chromone inhibitor stigmatellin - binding to the ubiquinol oxidation center at the C-side of the mitochondrial membrane. *FEBS Lett.* 185, 311–315.
40. Lancaster, C.R.D. & Michel. H. (1996). New insights into the X-ray structure of the reaction center from *Rhodopseudomonas viridis*. In *Reaction centers of photosynthetic bacteria* (Michel-Beyerle, M.E., ed.), Springer-Verlag, Berlin, in press.
41. Sakabe, N. (1983). A focusing Weissenberg camera with multi-layer-line screens for macromolecular crystallography. *J. Appl. Cryst.* 16, 542–547.
42. Otwinowski, Z. (1993). DENZO. In *Data Collection and Processing*. (Sawyer, L., Isaacs, N. & Bailey, S., eds), pp. 56–62, SERC Daresbury Laboratory, Warrington, UK.
43. Otwinowski, Z. (1991). Maximum likelihood refinement of heavy atom parameters. In *Isomorphous Replacement and Anomalous Scattering*. (Wolf, W., Evans, P.R. & Leslie, A.G.W., eds), pp. 80–86, SERC Daresbury Laboratory, Warrington, UK.
44. Cowtan, K.D. (1994). 'DM': An automated procedure for phase improvement by density modification. *Joint CCP4 and ESF-EACBM Newsletter on Protein Crystallography* 31, 34–38.
45. Abrahams, J.P. & Leslie, A.G.W. (1996). Method used in the structural determination of bovine mitochondrial F1 ATPase. *Acta Cryst. D* 52, 30–42.
46. Jones, T.A., Zou, J.Y., Cowan, S.W. & Kjeldgaad, M. (1991). Improved methods for building models in electron density maps and the location of errors in these models. *Acta Cryst. A* 47, 110–119.
47. Brünger, A.T., Kuriyan, J. & Karplus, M. (1987). Crystallographic R-factor refinement by molecular dynamics. *Science* 235, 458–460.
48. Kraulis, P.J. (1991). MOLSCRIPT: a program to produce both detailed and schematic plots of protein structures. *J. Appl. Cryst.* 24, 946–950.
49. Merrit, E.A. & Murphy, M.E.P. (1994). Raster3D Version 2.0. A program for photorealistic molecular graphics. *Acta Cryst.* D 50, 869–873.
50. Nicholls, A., Sharp, K. & Honig, B. (1991). Protein folding and association: insights from the interfacial and thermodynamic properties of hydrocarbons. *Proteins* 11, 281–296.